

Roles of heating and helicity in ultrafast all-optical magnetization switching in TbFeCo

Xianyang Lu,^{1,2} Xiao Zou,¹ Denise Hinzke,³ Tao Liu,⁴ Yichuan Wang,^{1,2} Tuyuan Cheng,⁵ Jing Wu,^{1,2,*} Thomas A. Ostler,^{6,7} Jianwang Cai,^{4,†} Ulrich Nowak,³ Roy W. Chantrell,¹ Ya Zhai,^{5,8} and Yongbing Xu^{2,5,‡}

¹*Department of Physics, University of York, York, YO10 5DD, UK*

²*York-Nanjing International Joint Center in Spintronics,*

School of Electronic Science and Engineering, Nanjing University, Nanjing, 210093, China

³*Fachbereich Physik, Universität Konstanz, 78457 Konstanz, Germany*

⁴*Institute of Physics, Chinese Academy of Sciences, Beijing 100190, China*

⁵*Spintronics and Nanodevice Laboratory, Department of Electronics, University of York, York YO10 5DD, UK*

⁶*Faculty of Arts, Computing, Engineering and Sciences, Sheffield Hallam University, Sheffield, S1 1WB, UK*

⁷*Département de Physique, L'Université de Liège, B-4000 Liège, Belgium*

⁸*Department of Physics, Southeast University, Nanjing, 210096, China*

(Dated: November 28, 2017)

Using time-resolved magneto-optical Kerr effect (TR-MOKE) method, helicity-dependent all-optical magnetization switching (HD-AOS) is observed in ferrimagnetic TbFeCo films. The thermal effect and opto-magneto effects are separately justified after single circularly polarized laser pulse. The integral evolution of this ultrafast switching is characterized on different time scales and the defined magnetization reversal time of 460 fs is the fastest ever observed. Combining the heat effect and inverse Faraday effect (IFE), micromagnetic simulations based on a single macro-spin model are performed that reproduce HD-AOS following a linear reversal mechanism.

Since the magnetization was demonstrated to be reversed by a femtosecond laser pulse without any external magnetic field [1], this all-optical switching (AOS) has been extensively studied in recent years. All-optical manipulation of magnetism becomes attractive due to its potential technological applications [2, 3]. AOS in the ferrimagnetic GdFeCo alloy, the initially investigated material for AOS, is demonstrated to be a pure laser-induced thermal effect [4–6] via a transient ferromagnetic-like state [7]. Very recently, ultrafast electronic heat currents have been shown experimentally to be sufficient to switch the magnetization in GdFeCo [8, 9] which further verifies the thermal origin of AOS in GdFeCo [10]. Consequently, AOS in GdFeCo is independent to the circular helicity of laser pulses, which is named as helicity-independent AOS (HI-AOS).

On the other hand, AOS observed in other materials is determined by the laser helicity such as ferromagnetic Co/Pt multilayers [11], FePt nanoparticles [12], synthetic ferrimagnetic heterostructures [13] and Tb-based ferrimagnets [14–16]. The polarization of the incident circularly polarized laser pulse plays a significant role in this helicity-dependent AOS (HD-AOS) to determine the magnetization orientation. HD-AOS is also observed in GdFeCo for a narrow range of fluence [17], which was quantitatively explained by magnetic circular dichroism (MCD) [18]. However, the underlying physics of HD-AOS in a larger variety of materials is still unclear, especially of the role of the circularly polarized laser. Several experimental criterions and models have been proposed to interpret the HD-AOS. A so-called low-remnance criterion was reported that HD-AOS is only obtained below

a magnetization remanence threshold of 220 emu/cm^3 for a number of materials [15]. This remanence threshold is affected by the temperature-dependent change of static magnetic properties induced by accumulative heat from laser pulses. Recently, a domain size criterion for the observation of HD-AOS has been proposed, whereby the laser spot size should be smaller than the equilibrium size of magnetic domains forming during the cooling process after laser irradiation [19]. Meanwhile, using a time-dependent anomalous Hall effect technique, HD-AOS has been demonstrated to consist of a steplike helicity-independent multiple-domain formation followed by a helicity-dependent remagnetization. Thermal and opto-magnetic effects are separately identified under the irradiation of consecutive laser pulses in a discontinuously way [20]. In all the models or experimental conditions, laser-induced heat or the accumulative heat plays a significant role. Specifically, thermally demagnetization by multiple laser pulses is emphasized in Ref. 20. In this context, a question is intuitively brought out: can the thermal and opto-magnetic effects be obtained simultaneously during a single circularly polarized laser pulse? The ultrafast laser-induced demagnetization is a well-known thermally induced process after laser pulse irradiation [21] and the interplay between thermal and optical effects during one single laser pulse seems feasible. However, in all the Kerr or Faraday image detections, it is impossible to justify both of these two effects because only the final static magnetization states are observed.

To explore the roles of the thermal effect and laser helicity in HD-AOS and the time scales in this process, we used the ultrafast laser pump-probe technique, also

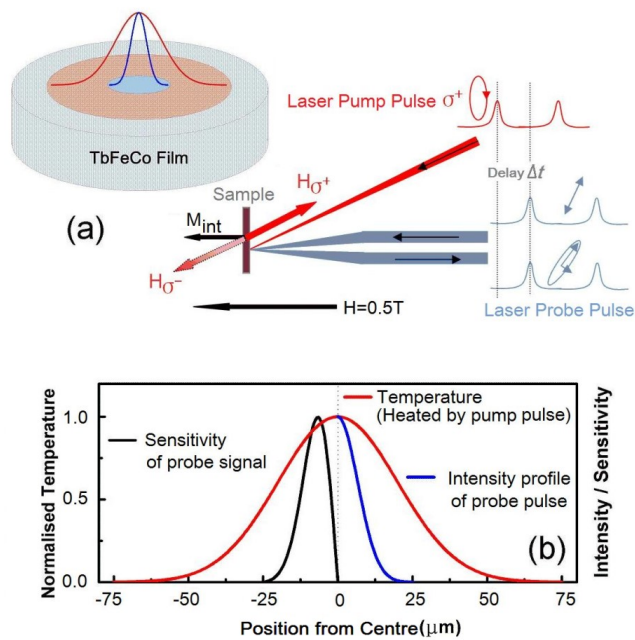


FIG. 1. (a) a schematic diagram of the experimental setup with a bias field $H = 0.5$ T. H_{σ^+} represents the opto-magnetic field of the pump pulse of σ^+ polarization (red line) via the IFE. The direction of H_{σ^-} would switch by 180° . (b) the normalized radial sensitivity of Kerr rotation (only left half shown for clarity) and temperature distribution across the pump spot together with the intensity profile of the probe spot (only right half shown for clarity).

known as time-resolved magneto-Kerr effect measurement [22], to measure the transient magnetization change after single laser pulse irradiation in TbFeCo. The transient reflectivity change is also monitored in the same time. TbFeCo is a very similar ferrimagnet compared to GdFeCo in so much as the Tb sublattice is antiferromagnetically coupled with the FeCo sublattice [23–25]. However, because of the large difference between the spin-orbit coupling of Tb and Gd [26], Gd- and Tb- based alloys show different ultrafast spin dynamics as well as a distinct switching mechanisms [27]. Also, with a large coercive field, TbFeCo is suitable for magnetic recording applications [28].

A 20 nm $\text{Tb}_{19}\text{Fe}_{66}\text{Co}_{15}$ thin film was deposited on a Corning 7059 glass substrates with a 20 Å Ta underlayer at ambient temperature using dc magnetron sputtering. A composite target, made by symmetrical placement of Tb and Co chips on the Fe target, is adopted to deposit TbFeCo films with a composition determined by inductively coupled plasma-atomic emission spectroscopy (ICP-AES). Sputtering rates for TbFeCo and Ta are about 0.9 and 1.1 Å/s, respectively. The TbFeCo film is covered by a 40 Å Au layer to protect against oxidation. The TbFeCo film exhibits a strong perpendicular anisotropy with a coercive field of 0.39 T measured by

vibrating sample magnetometry (VSM) at room temperature (see Fig. S2 in Supplemental Materials).

A typical polar TR-MOKE setup is used for all-optical pump-probe measurements. An ultrafast regenerative Ti:sapphire laser system with pulse width 150 fs, central wavelength 800 nm, and repetition rate of 1 kHz was used. The polarization of the 800 nm pump beam is varied between linear and circular using a $\lambda/4$ waveplate while the polarization of the 400 nm probe beam remains linear. The pump pulses are incident onto the sample at 10 degrees to the sample normal and the probe pulses at normal incidence. Both pump and probe beam are focused onto the same spot on the sample using two lenses with different focal length and positioned with the help of a CCD camera. The spot diameter is around 150 μm for the pump and 50 μm for the probe. The normalized intensity of the pump and probe beams can be described by a Gaussian distribution. Assuming the sensitivity is proportional to the beam intensity and the probing area, the probe sensitivity is calculated as shown in Fig. 1(b). The probe is sensitive to a wide range of temperatures and most sensitive to materials in the temperature range from 80 to 97 % of the peak temperature at the centre of the pump/probe. The temporal overlap of the laser pump pulse and the laser probe pulse is found to be about 250 fs FWHM. The rotation of the polarization and change of the reflectivity of the reflected probe beam is detected. To maintain the same initial magnetic state, a magnetic field $H_{ext} = 0.5$ T, which is 0.1 T higher than the sample coercive field at room temperature, is applied perpendicular to the sample plane.

In order to separate thermal and opto-magnetic contributions, time domain measurements are performed, varying laser pump fluence and helicity while keeping the direction of an external magnetic field fixed in the direction almost parallel to the direction of the magnetization induced due to the σ^- helicity (and nearly anti-parallel in the σ^+ case) pulses. The transient Kerr rotation obtained under different laser fluences with different laser helicities are shown in Fig. 2(a-c). Between the two lower laser fluences (2.8 and 5 mJ/cm^2), the dynamic responses are very similar except that the amplitude is increased with the laser fluence. The two curves taken with different laser helicity converge after around 240 fs time delay, suggesting that only thermal effects exist for these laser fluences because the thermal effects are insensitive to the laser helicity while the opto-magnetic (nonthermal) effect is. The peaks around zero delay are the so-called specular inverse Faraday effect (SIFE) and specular optical Kerr effect (SOKE) contributions [29], as detailed in Fig. S1 in the Supplemental Materials. However, as the laser fluence is increased to 9 mJ/cm^2 , the two curves taken with different laser helicity no longer converge. The curve excited by laser pulses of σ^+ polarization, a helicity opposite to the external magnetic field, switches further away from the initial magnetization direction compared

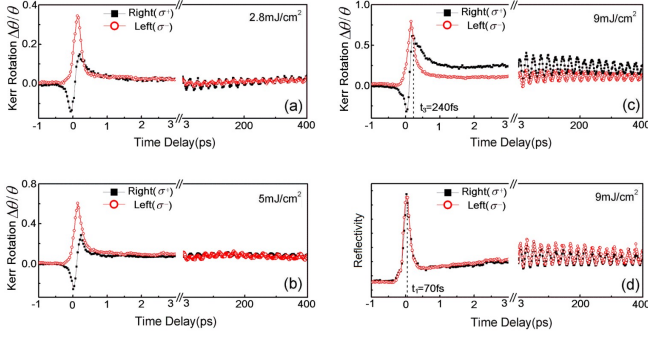


FIG. 2. (a) and (b) show the time domain Kerr rotation taken under 2.8 and 5 mJ/cm² pump fluence. (c) presents the time domain Kerr rotation obtained under pump beam fluence 9 mJ/cm². At about 240 fs time delay, the curve excited by pump pulses of σ^+ polarization (black solid squares) starts to switch further away from the initial magnetization direction compared with the curve excited by σ^- polarized (red hollow dots) pump pulses. (d) shows the time domain reflectivity data at 9 mJ/cm² for both σ^+ and σ^- polarization. The two curves overlap with the peak at $t_1 = 70$ fs, indicating the maximal electron temperature.

to the curve excited by σ^- polarised laser pulses. This extra switching starts at $t_3 = 240$ fs, indicating the onset of the opto-magnetic effect. The time evolution of the reflectivity has also been investigated indicating a peak electron temperature at $t_1 = 70$ fs. There is no obvious laser helicity dependence in the reflectivity which can be seen from the data taken at 9 mJ/cm² as shown in Fig. 2(d). In this case, the absorptions of light are at the same level as well as the electron temperature profiles which means there is no significant MCD effect.

The thermal and nonthermal effects on the magnetization can be separated by analysing respectively the sum and difference of the experimental data under different laser helicities. The data in Fig. 2(a-c) have been analysed accordingly and are presented in Fig. 3(a-b). The difference data in Fig. 3(a) shows the time evolution of the nonthermal effect. For the two cases with lower laser fluence, the time evolution of the nonthermal effect overlaps and goes back to its original state immediately after the SIFO/SOKE peak, giving no indication of any opto-magnetic effect. As the pump fluence is increased to 9 mJ/cm², the difference signal does not return to the original state immediately. Instead it keeps increasing to its maximum magnitude at $t_4 = 460$ fs time delay showing that the magnetization has switched in partial regions of the irradiated area to a different magnetization state. This demonstrates unambiguously an opto-magnetic switching in TbFeCo triggered at $t_3 = 240$ fs and magnetization re-orientation at $t_4 = 460$ fs after circularly polarized laser excitation.

Fig. 3(b) presents the time evolution of the directly measured heat-driven dynamics excited by the linearly

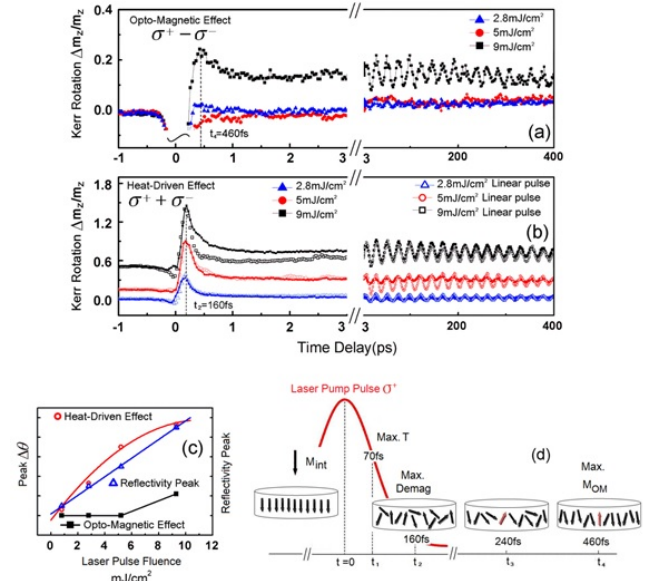


FIG. 3. (a) shows the difference between the time domain under σ^+ and σ^- pump pulses. (b) The three solid curves show the sum of the time domain data under σ^+ and σ^- pump pulses. The hollowed curves are time domain responses excited by the linearly polarized laser pulse at the same pump fluences. (c) The peak amplitude of the heat-driven effect (red circles), of the reflectivity (blue crosses), and of the opto-magnetic effect (black dots) at a delay time of 460 fs as a function of the pump fluence. (d) Shows a schematic diagram on ultrafast process induced at 9 mJ/cm² pump fluence.

polarized laser of the same pulse energy along with the data obtained by taking the sum of the σ^+ and σ^- data for three different laser fluences. All three pairs of time domain Kerr rotation reach maxima around $t_2 = 160$ fs, indicating the time scale of the magnetic order quenching. Two pairs of time domain data taken at lower laser fluence overlap with each other extremely well since the SIFE/SOKE changes phase between σ^+ and σ^- helicity and are thus cancelled out by the sum operation. The pair taken at 9 mJ/cm² start to diverge from each other immediately after the maximum demagnetization with the sum data deviating further from the initial magnetization state, indicating the onset of the opto-magnetic effects excited by σ^+ pump pulses, which are more profound than those excited by the σ^- . This is expected since the opto-magnetic effect induced by two different laser helicities are different in phase as well as in magnitude depending on the instantaneous magnetization state, and also supported by theoretical calculations to be shown later. The peak amplitude of the thermal and reflectivity data is plotted as a function of the pump laser fluence in Fig. 3(c) together with the amplitude of the nonthermal data at 460 fs time delay. Fig. 3(c) shows that the electron temperature is proportional to the laser fluence; the sample is nearly totally demagnetized at 9 mJ/cm² which is consistent with the precondition re-

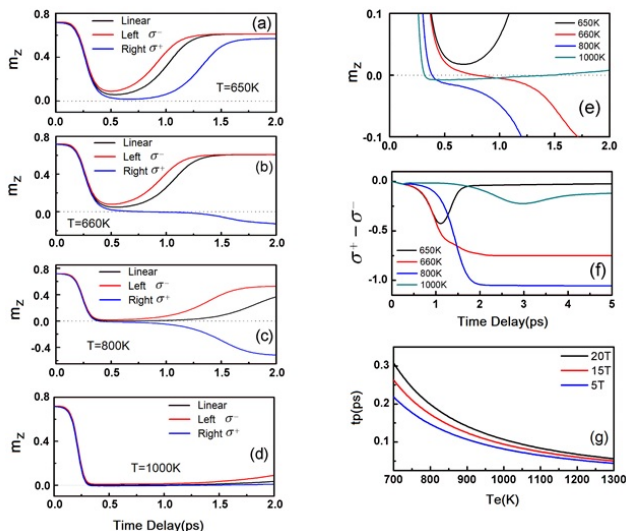


FIG. 4. (a-d) Magnetic response for increasing peak electron temperatures showing the onset of the magnetization reversal. Reversal occurs at around 660 K, where the linear reversal mechanism sets in. At higher temperature (d) the magnetization is destroyed after reversal. (e) magnetic response M_z for different values of the peak electron temperature. (f) shows the difference in the response to the difference helicities. Optically induced reversal is demonstrated at 660 and 800 K. The onset of reversal depends critically on the onset of linear reversal. The response time calculated from Eq. S1 demonstrates that the predicted reversal takes place on the sub-picosecond timescale, consistent with the experimental results. (g) Minimal field and temperature pulse time needed to trigger a magnetization reversal taken from Eq. S1.

quired for helicity-dependent switching [20]; there is no sign of an opto-magnetic effect for data taken at lower pump fluence. Note that 9 mJ/cm^2 is the highest pump fluence, which can be applied without damaging the sample surface, and the opto-magnetic effect is only observed at this highest pump fluence. The whole ultrafast process induced at 9 mJ/cm^2 pump fluence is schematically summarized in Fig. 3(d). The electron temperature reaches its maximum at 70 fs time delay and the magnetic order is largely quenched by 160 fs. The onset of opto-magnetic switching takes place within 240 fs and a new magnetization direction is defined by 460 fs.

To understand the observed time domain results of HD-AOS, two main effects are considered, namely the MCD [18] and the IFE [30]. MCD leads to a different absorption of the two circular helicities in the different domains and it is excluded because from the transient reflectivity change curves, no difference is observed with respect to the laser helicity. In Ref. 12, the magnetization induced through the IFE effect was directly calculated for the case of FePt with ab-initio methods [31]. In our simulations, due to a lack of ab-initio calculations for the considered TbFeCo alloy, this temporal change of the magnetization caused by the IFE is assumed to

be due to an effective magnetic field [17, 32]. Our simulations are based on a single macro-spin model solving the Landau-Lifshitz-Bloch (LLB) equation numerically [33–38], an equation of motion which takes into account transient changes in the length of the magnetization. All our methods are described in detail in Ref. 36 and also summarized in the Supplemental Materials. Results of these simulations are shown in Fig. 4(a-d) for different peak electron temperatures T_e , corresponding to different laser fluences, as summarised in Fig. 4(e-f). The figure focuses on the short time development of the easy axis component of the reduced magnetization (M/M_s). Starting with its room temperature equilibrium value of about 0.8, complete demagnetization can be triggered within 300 fs and magnetization reversal can be triggered within sub-picosecond time scales for higher T_e . The theoretical model reproduces the sub-picosecond reversal observed experimentally and confirms the above interpretation of the experimental data. The magnetic order is first quenched within 160 fs and a new magnetization direction is defined within 460 fs via a linear reversal mechanism without spin precession. Above all, the reversal occurs only above a critical temperature corresponding to that of the linear reversal model; reversal on this timescale cannot occur via precessional mechanisms. Therefore, the peak electron temperature plays a significant role in HD-AOS. In Ref. 39 an analytical formula was derived for the minimal pulse time (in terms of a rectangular field and temperature pulse), which is needed to switch the sign of the magnetization (see Eq. S1 in the Supplemental Materials). It is illustrated in Fig. 3(g). We noticed that in the simulations the switching times are slightly larger than what the analytical formula suggested. This is due to the fact that for the formula a rectangular temperature and field pulse is assumed while in the simulations more realistic profiles are calculated. We also note that the simulations further predict a rapid increase of the magnetization in a negative sense after reversal, whereas the experimental data indicate that the magnetization recovers towards the original value. It is likely due to the simplified nature of the calculations, based on a single spin, whereas the experimental sample has a large-scale domain structure. While the reversal of the magnetization via the linear reversal mechanism is unlikely to be affected by the domain structure, it is reasonable to expect that the magnetization after the pulse will be an effect which cannot be simulated within the current single spin model. Furthermore, multi-macrospin calculations would most likely still not be comparable with experimental measurements as the size of the probe beam is still many micrometres and likely beyond the size of this type of simulation.

In summary, the HD-AOS is unambiguously demonstrated in TbFeCo film by one single circularly polarized laser pulse. The thermal and opto-magnetic effects are seen to have different time scales, respectively.

High pump fluences are required for the effect of the laser helicity, which is consistent with other reported works [19, 20]. Note that the effect of accumulative heat is not excluded in our measurements, but the 1 kHz laser repetition rate is much lower than the repetition rate used in Ref. 15 which shows no significant accumulative heat. Besides, the reflectivity change relaxation time is quite small in our measurements so the effect of accumulative heat should not play a role. The interplay between laser heating and helicity is stimulated by a single laser pulse. The integral evolution using the TR-MOKE method including the time points when it comes peak electron temperature, fully demagnetized state, magnetization switching triggered and a new magnetization direction is defined. Furthermore, from the sub-picosecond time domain evolution of HD-AOS, the observed magnetic switching time in 460 fs is the fastest among the reported times [17, 32, 40, 41]. On the other hand, this sub-picosecond switching is reproduced using a single macro-spin model based on the stochastic Landau-Lifschitz-Bloch equation, confirming the linear reversal mechanism without spin precession in the all-optically induced magnetization switching. Also, the simulation suggests that heating the electrons system to a critical temperature may play an important role in this kind of magnetization reversal. Above all, the finding of the ultrafast helicity-dependent all-optical magnetization switching in a high anisotropy system triggered by single laser pulse brings all-optical magnetic recording a major step close to the high data rate and high data density applications.

This work was supported in part by the National Basic Research Program of China (No. 2014CB921101), National Key Research and Development Program of China (No. 2016YFA0300803), the National Natural Science Foundation of China (No. 61427812, 11574137, 11774160), Jiangsu Shuangchuang Programme and the Natural Science Foundation of Jiangsu Province of China (No. BK20140054). T. A. Ostler gratefully acknowledges the support of the Marie Curie incoming BeIPD-COFUND fellowship program at the University of Liège.

* Email: jing.wu@york.ac.uk

† Email: jwcai@iphy.ac.cn

‡ Email: yongbing.xu@york.ac.uk

- [1] C. D. Stanciu, F. Hansteen, A. V. Kimel, A. Kirilyuk, A. Tsukamoto, A. Itoh, and T. Rasing, *Phys. Rev. Lett.* **99**, 047601 (2007).
- [2] J. Y. Chen, L. He, J. P. Wang, and M. Li, *Phys. Rev. Applied* **7**, 021001 (2017).
- [3] Z. Al Azim, X. Fong, T. Ostler, R. Chantrell, and K. Roy, *IEEE Electron Device Lett.* **35**, 1317 (2014).
- [4] T. A. Ostler, J. Barker, R. F. L. Evans, R. W. Chantrell, U. Atxitia, O. Chubykalo-Fesenko, S. El Moussaoui, L. Le Guyader, E. Mengotti, L. J. Heyderman, F. Nolting, A. Tsukamoto, A. Itoh, D. Afanasiev, B. A. Ivanov, A. M. Kalashnikova, K. Vahaplar, J. Mentink, A. Kirilyuk, T. Rasing, and A. V. Kimel, *Nat. Commun.* **3**, 666 (2012).
- [5] A. Kirilyuk, A. V. Kimel, and T. Rasing, *Rep. Prog. Phys.* **76**, 026501 (2013).
- [6] R. Chimata, L. Isaeva, K. Kádas, A. Bergman, B. Sanyal, J. H. Mentink, M. I. Katsnelson, T. Rasing, A. Kirilyuk, A. Kimel, O. Eriksson, and M. Pereiro, *Phys. Rev. B* **92**, 094411 (2015).
- [7] I. Radu, K. Vahaplar, C. Stamm, T. Kachel, N. Pontius, H. A. Dürr, T. A. Ostler, J. Barker, R. F. L. Evans, R. W. Chantrell, A. Tsukamoto, A. Itoh, A. Kirilyuk, T. Rasing, and A. V. Kimel, *Nature(London)* **472**, 205 (2011).
- [8] R. B. Wilson, J. Gorchon, Y. Yang, C.-H. Lambert, S. Salahuddin, and J. Bokor, *Phys. Rev. B* **95**, 180409 (2017).
- [9] Y. Xu, M. Deb, G. Malinowski, M. Hehn, W. Zhao, and S. Mangin, *Adv. Mater.* , 1703474 (2017).
- [10] U. Atxitia, T. A. Ostler, R. W. Chantrell, and O. Chubykalo-Fesenko, *Appl. Phys. Lett.* **107**, 192402 (2015).
- [11] C.-H. Lambert, S. Mangin, B. S. D. C. S. Varaprasad, Y. K. Takahashi, M. Hehn, M. Cinchetti, G. Malinowski, K. Hono, Y. Fainman, M. Aeschlimann, and E. E. Fullerton, *Science* **345**, 1337 (2014).
- [12] R. John, M. Berritta, D. Hinzke, C. Müller, T. Santos, H. Ulrichs, P. Nieves, J. Walowski, R. Mondal, O. Chubykalo-Fesenko, J. McCord, P. M. Oppeneer, U. Nowak, and M. Münzenberg, *Sci. Rep.* **7**, 4114 (2017).
- [13] S. Mangin, M. Gottwald, C.-H. Lambert, D. Steil, V. Uhlir, L. Pang, M. Hehn, S. Alebrand, M. Cinchetti, G. Malinowski, Y. Fainman, M. Aeschlimann, and E. E. Fullerton, *Nat. Mater.* **13**, 286 (2014).
- [14] A. Hassdenteufel, B. Hebler, C. Schubert, A. Liebig, M. Teich, M. Helm, M. Aeschlimann, M. Albrecht, and R. Bratschitsch, *Adv. Mater.* **25**, 3122 (2013).
- [15] A. Hassdenteufel, J. Schmidt, C. Schubert, B. Hebler, M. Helm, M. Albrecht, and R. Bratschitsch, *Phys. Rev. B* **91**, 104431 (2015).
- [16] T. Y. Cheng, J. Wu, M. Willcox, T. Liu, J. W. Cai, R. W. Chantrell, and Y. B. Xu, *IEEE Trans. Magn.* **48**, 3387 (2012).
- [17] K. Vahaplar, A. M. Kalashnikova, A. V. Kimel, S. Gerlach, D. Hinzke, U. Nowak, R. Chantrell, A. Tsukamoto, A. Itoh, A. Kirilyuk, and T. Rasing, *Phys. Rev. B* **85**, 104402 (2012).
- [18] A. R. Khorsand, M. Savoini, A. Kirilyuk, A. V. Kimel, A. Tsukamoto, A. Itoh, and T. Rasing, *Phys. Rev. Lett.* **108**, 127205 (2012).
- [19] M. S. El Hadri, M. Hehn, P. Pirro, C.-H. Lambert, G. Malinowski, E. E. Fullerton, and S. Mangin, *Phys. Rev. B* **94**, 064419 (2016).
- [20] M. S. El Hadri, P. Pirro, C.-H. Lambert, S. Petit-Watelot, Y. Quessab, M. Hehn, F. Montaigne, G. Malinowski, and S. Mangin, *Phys. Rev. B* **94**, 064412 (2016).
- [21] E. Beaurepaire, J.-C. Merle, A. Daunois, and J.-Y. Bigot, *Phys. Rev. Lett.* **76**, 4250 (1996).
- [22] B. Liu, X. Ruan, Z. Wu, H. Tu, J. Du, J. Wu, X. Lu, L. He, R. Zhang, and Y. Xu, *Appl. Phys. Lett.* **109**, 042401 (2016).
- [23] S. Alebrand, M. Gottwald, M. Hehn, D. Steil, M. Cinchetti, D. Lacour, E. E. Fullerton, M. Aeschlimann, and S. Mangin, *Appl. Phys. Lett.* **101**, 162408

- (2012).
- [24] A. Hassdenteufel, C. Schubert, J. Schmidt, P. Richter, D. R. T. Zahn, G. Salvan, M. Helm, R. Bratschitsch, and M. Albrecht, *Appl. Phys. Lett.* **105**, 112403 (2014).
- [25] R. Moreno, T. A. Ostler, R. W. Chantrell, and O. Chubykalo-Fesenko, *Phys. Rev. B* **96**, 014409 (2017).
- [26] M. Wietstruk, A. Melnikov, C. Stamm, T. Kachel, N. Pontius, M. Sultan, C. Gahl, M. Weinelt, H. A. Dürr, and U. Bovensiepen, *Phys. Rev. Lett.* **106**, 127401 (2011).
- [27] A. R. Khorsand, M. Savoini, A. Kirilyuk, A. V. Kimel, A. Tsukamoto, A. Itoh, and T. Rasing, *Phys. Rev. Lett.* **110**, 107205 (2013).
- [28] C. Bunce, J. Wu, G. Ju, B. Lu, D. Hinzke, N. Kazantseva, U. Nowak, and R. W. Chantrell, *Phys. Rev. B* **81**, 174428 (2010).
- [29] F. Dalla Longa, J. T. Kohlhepp, W. J. M. De Jonge, and B. Koopmans, *Phys. Rev. B* **75**, 224431 (2007).
- [30] T. D. Cornelissen, R. Córdoba, and B. Koopmans, *Appl. Phys. Lett.* **108**, 142405 (2016).
- [31] M. Battiato, G. Barbalinardo, and P. M. Oppeneer, *Phys. Rev. B* **89**, 014413 (2014).
- [32] K. Vahaplar, A. M. Kalashnikova, A. Kimel, D. Hinzke, U. Nowak, R. Chantrell, A. Tsukamoto, A. Itoh, A. Kirilyuk, and T. Rasing, *Phys. Rev. Lett.* **103**, 117201 (2009).
- [33] D. A. Garanin and O. Chubykalo-Fesenko, *Phys. Rev. B* **70**, 212409 (2004).
- [34] D. A. Garanin and E. M. Chudnovsky, *Phys. Rev. B* **56**, 11102 (1997).
- [35] U. Atxitia, O. Chubykalo-Fesenko, N. Kazantseva, D. Hinzke, U. Nowak, and R. W. Chantrell, *Appl. Phys. Lett.* **91**, 232507 (2007).
- [36] N. Kazantseva, D. Hinzke, U. Nowak, R. W. Chantrell, U. Atxitia, and O. Chubykalo-Fesenko, *Phys. Rev. B* **77**, 184428 (2008).
- [37] T. A. Ostler, M. O. A. Ellis, D. Hinzke, and U. Nowak, *Phys. Rev. B* **90**, 094402 (2014).
- [38] U. Atxitia, D. Hinzke, and U. Nowak, *J. Phys. D: Appl. Phys.* **50**, 033003 (2017).
- [39] N. Kazantseva, D. Hinzke, R. W. Chantrell, and U. Nowak, *EPL* **86**, 27006 (2009).
- [40] L. Le Guyader, M. Savoini, S. El Moussaoui, M. Buzzi, A. Tsukamoto, A. Itoh, A. Kirilyuk, T. Rasing, A. V. Kimel, and F. Nolting, *Nat. Commun.* **6**, 5839 (2015).
- [41] T. Ogasawara, N. Iwata, Y. Murakami, H. Okamoto, and Y. Tokura, *Appl. Phys. Lett.* **94**, 162507 (2009).